

Effect of Solid Subcooling on Natural Convection Melting of a Pure Metal

C. Beckermann

Department of Mechanical Engineering,
The University of Iowa,
Iowa City, IA 52242

R. Viskanta

Heat Transfer Laboratory,
School of Mechanical Engineering,
Purdue University,
West Lafayette, IN 47907

A combined experimental and numerical study is reported of melting of a pure metal inside a vertical rectangular enclosure with natural convection in the liquid and conduction in the solid. The numerical model is successfully verified by conducting a series of experiments covering a wide range of hot and cold wall temperatures. It is found that solid subcooling significantly reduces the melting rate when compared to melting with the solid at the fusion temperature. Because the cooled wall is held below the fusion temperature of the metal, the solid/liquid interface eventually reaches a stationary position. For moderate values of the subcooling parameter the steady-state interface is almost vertical and parallel to the cold wall. Strong subcooling results in an early termination of the melting process, such that natural convection in the relatively small liquid region cannot fully develop. For moderate subcooling, correlations have been derived for the steady-state volume and heat transfer rates. While many aspects of melting with solid subcooling appear to be similar to ordinary nonmetallic solids, important differences in the local flow structures and heat transfer mechanisms are observed.

Introduction

Solid/liquid phase change in enclosures with natural convection in the liquid phase has recently received considerable research attention (Viskanta, 1985) due to its large number of applications, including latent heat storage, materials processing, crystal growth, casting of metals, purification of materials, and others. The effects of natural convection in the melt on the phase-change process are now well understood for certain geometries and medium to high Prandtl number fluids (Viskanta, 1985). Despite its importance in many industrial applications, melting or solidification of metals with natural convection in the liquid phase has received only little research attention. Experiments with lead (Szekely and Chhabra, 1970), mercury (Chiesa and Guthrie, 1974), gallium (Gau and Viskanta, 1986), and tin (Wolff and Viskanta, 1987) have demonstrated, however, that natural convection can considerably affect the solid/liquid interface shape and motion during phase change of low Prandtl number fluids. This has also been confirmed by numerical studies of melting of pure metals from a vertical wall (Webb and Viskanta, 1986; Wolff and Viskanta, 1987).

In all previous studies of melting of metals in enclosures, heat conduction in the solid phase is not considered. While natural convection in the melt increases the melting rate, subcooling of the solid acts to decrease the melting rate because of heat extraction through the solid away from the solid/liquid interface. If the cooled wall is held below the fusion temperature of the metal, the melting process can be completely terminated and the system will reach a steady state where the convective heat transfer from the melt to the interface is balanced by the heat conduction through the solid. The combined effects of natural convection in the liquid and heat conduction in the solid have been studied for melting of ordinary nonmetallic solids in rectangular enclosures (Benard et al., 1986; Kassinos and Prusa, 1986). While Benard and co-workers report the results of only one test case, Kassinos and Prusa present numerical results for the interface positions and/or melt volumes of two cases with solid subcooling. Because of the high thermal conductivity of metals, heat con-

duction in the solid can, however, be expected to exert an even stronger influence on melting of metals.

The purpose of the present study is to examine the influence of heat conduction in the solid phase of a pure metal during melting driven by natural convection in the melt. A series of experiments is performed in a rectangular enclosure heated and cooled at two opposite vertical side walls using gallium as the phase-change material. Measurements of the temperature distributions and interface positions are utilized to infer the heat transfer and melting phenomena for a variety of hot and cold wall temperature combinations. The experiments are supplemented by numerical simulations of the various test cases. The numerical results are validated through comparisons with the experimental data.

Analysis

Model Equations. The physical system considered in the present study is shown in Fig. 1. The vertical side walls of the enclosure are of height H and maintained at uniform temperatures, while the connecting horizontal walls of length L are considered adiabatic. Initially, the solid metal and the vertical sidewalls are at a uniform temperature, T_C , that is below the fusion temperature, i.e., $T_C < T_f$. At time $t=0$, the melting process is initiated by raising impulsively the left vertical sidewall temperature to T_H , where $T_H > T_f$.

In the present model, the flow is assumed to be laminar, incompressible, and two-dimensional, and the Boussinesq approximation is invoked. The thermophysical properties are assumed constant, but may be different for the liquid and solid phases. Because of the small Stefan numbers encountered in the present study (see Experiments), normal velocities at the solid/liquid interface due to density change upon melting can be neglected (Prusa and Yao, 1985; Kassinos and Prusa, 1986). With the foregoing assumptions, the mass, momentum, and energy conservation equations for the liquid and solid phases can be written in dimensionless form (see Nomenclature) as

Liquid:

$$\nabla \cdot \mathbf{u} = 0 \quad (1)$$

$$\frac{\partial \mathbf{u}}{\partial Fo} + (\mathbf{u} \cdot \nabla) \mathbf{u} = -\nabla p + \text{Pr} \nabla^2 \mathbf{u} + \text{Ra} \text{Pr} \theta_j \mathbf{e}_j \quad (2)$$

Contributed by the Heat Transfer Division for publication in the JOURNAL OF HEAT TRANSFER. Manuscript received by the Heat Transfer Division May 24, 1988. Keywords: Liquid Metals, Natural Convection, Phase-Change Phenomena.

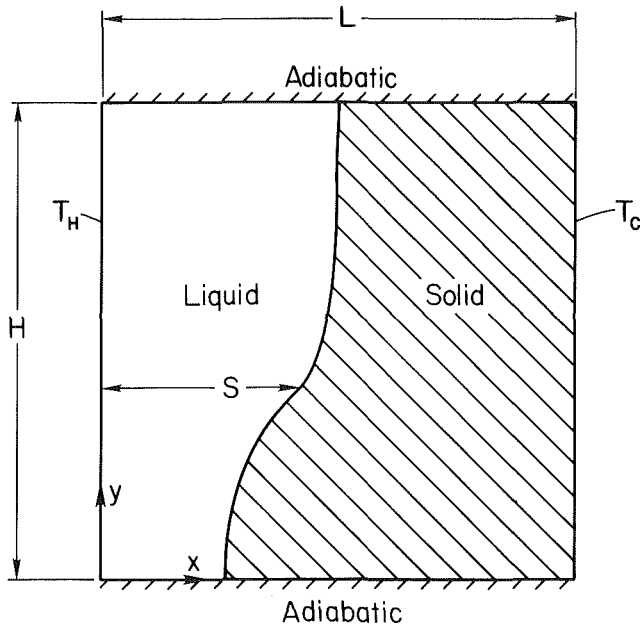


Fig. 1 Schematic of the physical model and coordinate system

$$\frac{\partial \theta_l}{\partial Fo} + \mathbf{u} \cdot \nabla \theta_l = \nabla^2 \theta_l \quad (3)$$

Solid:

$$\frac{\partial \theta_s}{\partial Fo} = \alpha^* \nabla^2 \theta_s \quad (4)$$

The initial and boundary conditions for the present system may be stated as

Initial Conditions ($Fo < 0$):

$$s = 0, \quad \theta_s = -1 \quad (5)$$

Boundary Conditions ($Fo \geq 0$):

$$\mathbf{u} = 0, \quad \theta_l = 1 \quad \text{at } \xi = 0, \quad 0 \leq \eta \leq A$$

$$\mathbf{u} = 0, \quad \theta_s = -1 \quad \text{at } \xi = 1, \quad 0 \leq \eta \leq A \quad (6)$$

$$\mathbf{u} = 0, \quad \frac{\partial \theta_l \text{ or } s}{\partial \eta} = 0 \quad \text{at } \eta = 0 \text{ or } A, \quad 0 \leq \xi \leq 1$$

In addition, the conditions at the solid/liquid interface, $\xi = s(\eta, Fo)$, are given by

$$\mathbf{u} = 0$$

$$\theta_s = \theta_l = 0 \quad (7)$$

$$k^* S_T (\nabla \theta_s \cdot \mathbf{n}) - (\nabla \theta_l \cdot \mathbf{n}) = \frac{\rho^*}{Ste} V_n$$

The dimensionless equations (1) to (7) show that the present problem is governed by eight dimensionless parameters, namely, the Rayleigh (Ra), Prandtl (Pr), and Stefan (Ste) numbers, the aspect ratio A , the subcooling parameter S_T , as well as the property ratios k^* , ρ^* , and α^* . However, equations (7) indicate that $k^* S_T$ and ρ^*/Ste can, theoretically, be combined into single parameters, thereby reducing the number of dimensionless parameters to six. As is commonly done in the solid/liquid phase-change literature, all results in the present study will be presented as functions of a dimensionless time τ , defined as

$$\tau = Fo Ste \quad (8)$$

With the above scaling of the Fourier number and in the limit of small Stefan numbers ($Ste \rightarrow 0$) the solution does not depend explicitly on the Stefan number. For the range of Stefan numbers considered in this study ($Ste < 0.08$), the above statement represents a good approximation. Consequently, the user of the dimensionless time τ will aid in the presentation of the results, although the present calculations are performed for finite Stefan numbers (see also the next section).

Note that the temperatures in the liquid and solid are non-dimensionalized using the temperature differences $\Delta T_l = T_H - T_f$ and $\Delta T_s = T_f - T_C$, respectively. Consequently, the dimensionless temperatures are limited to values between 0 and 1 in the liquid and 0 and -1 in the solid. With $S_T = \Delta T_s / \Delta T_l$, the subcooling parameter is equal to zero for no subcooling of the solid ($T_C = T_f$), and is limited to values greater than zero.

The results for the average heat transfer rates at the vertical side walls bounding the liquid and solid will be presented in terms of average Nusselt numbers defined as

$$\overline{Nu}_l = -\frac{1}{A} \int_0^A \frac{\partial \theta_l}{\partial \xi} d\eta \quad \text{at } \xi = 0$$

Nomenclature

A = aspect ratio = H/L	position = S/L	α^* = thermal diffusivity ratio = α_s/α_l
c = specific heat, J/kg K	S = interface position, m	β = coefficient of thermal expansion, 1/K
Fo = Fourier number = $t\alpha_l/L^2$	S_T = subcooling parameter = $\Delta T_s/\Delta T_l$	η = dimensionless vertical coordinate = y/L
g = gravitational acceleration, m/s ²	Ste = Stefan number = $c_l \Delta T_l / h_f$	θ_l = dimensionless liquid temperature = $(T_l - T_f) / \Delta T_l$
h = convective heat transfer coefficient, W/m ² K	t = time, s	θ_s = dimensionless solid temperature = $(T_s - T_f) / \Delta T_s$
h_f = latent heat of fusion, J/kg	T = temperature, K	ν = kinematic viscosity, m ² /s
H = height of enclosure, m	ΔT_l = temperature difference across liquid = $T_H - T_f$, K	ξ = dimensionless horizontal coordinate = x/L
k = thermal conductivity, W/mK	ΔT_s = temperature difference across solid = $T_f - T_C$, K	ρ = density, kg/m ³
k^* = thermal conductivity ratio = k_s/k_l	\mathbf{u} = dimensionless velocity = UL/α_l	ρ^* = density ratio = ρ_s/ρ_l
L = length of enclosure, m	\mathbf{U} = velocity, m/s	τ = dimensionless time = $Fo Ste$
\mathbf{n} = normal unit vector	v_n = dimensionless normal interface velocity = $V_n L / \alpha_l$	
Nu = Nusselt number = hL/k_l	V = dimensionless melt volume, see equation (10)	
P = pressure, Pa	V_n = normal interface velocity, m/s	
p = dimensionless pressure = $PL/\rho_l \alpha_l^2$	x = horizontal coordinate, m	
Pr = Prandtl number = ν_l/α_l	y = vertical coordinate, m	
Ra = Rayleigh number = $g\beta \Delta T_l L^3 / \nu_l \alpha_l$	α = thermal diffusivity, m ² /s	
s = dimensionless interface		

Subscripts

C = cold wall
f = fusion
H = hot wall
l = liquid
s = solid

$$\overline{\text{Nu}}_s = -\frac{k^* S_T}{A} \int_0^A \frac{\partial \Theta_s}{\partial \xi} d\eta \quad \text{at } \xi = 1 \quad (9)$$

According to the above equations, the heat transfer rates at both sidewalls ($\xi = 0$ and 1) are referenced to the heat transfer by conduction across the liquid region. At steady state (i.e., for a stationary solid/liquid interface), this will result in equal values of the Nusselt numbers at both side walls.

The temporal variation of the average solid/liquid interface location will be presented in terms of a dimensionless melt (liquid) volume defined as

$$V = \frac{1}{A} \int_0^A s d\eta \quad (10)$$

Solution Procedure. The movement and the irregular shape of the solid/liquid interface considerably complicate the numerical solution of the coupled equations (1) to (7). In the present study, a modified form of the implicit/explicit approach proposed by Sparrow and co-workers (Sparrow and Chuck, 1984; Sparrow and Ohkubo, 1986) is adopted for the treatment of the interface movement. The numerical solution proceeds through a series of small time intervals during which the solid/liquid interface is assumed to be fixed. For each such time interval, the field equations are solved by a fully *implicit* solution scheme (without neglecting the unsteady terms) in the now fixed liquid and solid domains. The solution of the field equations provides the energy fluxes at the interface after that time interval. The displacement of the interface can then be calculated *explicitly* (i.e., without iterations) from the interfacial energy balance, equation (7), and new solution domains are generated for the next time step. Since the interface displacement is performed at the end of the time interval, the present approach avoids complications in the formulation of the numerical solution scheme for the field equations due to a moving grid system (Sparrow and Ohkubo, 1986), as well as the iterative interaction of the temperature and velocity fields with the interface displacement (Sparrow and Chuck, 1984). The accuracy of this approach is demonstrated in the literature (Sparrow and Chuck, 1984; Sparrow and Ohkubo, 1986). It has been shown that for small Stefan numbers, the temperature and velocity fields are not strongly influenced by the movement of the interface (Prusa and Yao, 1985; Benard et al., 1986; Kassinos and Prusa, 1986). For the small Stefan numbers encountered in the present study (see Experiments), this effect is negligible. In the following, the numerical procedures for solving the field equations during each time interval are outlined.

The field equations (1) to (4), together with the boundary and initial conditions, equations (5) to (7), were solved utilizing a modified form of the control-volume-based discretization scheme described in detail elsewhere (Hsu, 1982; Webb and Viskanta, 1986). In this scheme, the field equations are integrated over discrete nonorthogonal control volumes. The additional terms due to the nonorthogonality of the grid are fully retained in the discretized equations. This is particularly important in view of the fact that for the conditions of the present study, the tilt ($\partial s / \partial \eta$) and curvature ($\partial^2 s / \partial \eta^2$) of the solid/liquid interface can be relatively large (see Results and Discussion and Yao, 1980). As mentioned previously, the present algorithm is based on an implicit discretization scheme for the unsteady terms in the field equations, without invoking the quasi-steady convection approximation (Benard et al., 1986; Webb and Viskanta, 1986). Other details of the computational sequence are essentially the same as in Hsu (1982) and do not need to be repeated here. The algorithm was considerably modified to facilitate the calculations to be performed simultaneously in the two domains (i.e., liquid and solid).

The highly irregular shapes of the liquid and solid domains were accommodated in the calculations by using a nonorthogonal curvilinear grid. After each movement of the interface new grids were algebraically generated utilizing a power-law clustering scheme (Webb and Viskanta, 1986). This procedure provides a high concentration of nodal points near the vertical boundaries and the solid/liquid interface where velocity and thermal boundary layers need to be accurately resolved. The nodal points were only slightly skewed in the η direction. In the calculations reported in the present study, grids of 26×26 nodal points were selected for the liquid and solid domains. It is realized that this relatively coarse grid might not be adequate to resolve all details of the flow structures in the liquid domain. The selected mesh size should only be viewed as a compromise between accuracy and computational cost. Additional tests of the accuracy of the numerical algorithm were performed for the limiting cases of melting of a pure substance without solid subcooling (Webb and Viskanta, 1986) and thermal natural convection in a square enclosure (DeVahl Davis and Jones, 1983) and good agreement with results reported in the literature was found.

The calculations were initialized by assuming the presence of a liquid layer of negligibly small thickness (i.e., $s < 0.01$). During the initial period of the simulation, a dimensionless time step of $\Delta \text{Fo} = 10^{-3}$ (~ 0.16 s) was utilized to assure a very small interface displacement. The time step was continually increased. Close to steady state, the time step was approximately equal to $\Delta \text{Fo} = 0.1$ (16 s). For each time step, the iterations were terminated when the dependent variables agreed to four significant figures at each nodal point and the residual source of mass was less than 1×10^{-5} . The numerical algorithm was partially vectorized and the calculations were performed on a CYBER 205 computer. A typical simulation of a melting process required a CPU time of about 1500 s in order to reach steady state.

Experiments

Experiments were performed in a well-insulated test cell of square cross section. The test cell had inside dimensions of 4.76 cm in height and width and 3.81 cm in depth. The relatively small size of the test cell was mainly dictated by the high price of the phase-change material (gallium). The horizontal bottom wall was constructed of a phenolic plate, while the top wall and the vertical front and back walls were made of Lexan. Both the phenolic plate and the Lexan have low thermal conductivities when compared to gallium. The two vertical side walls, which served as the heat source/sink, were multipass heat exchangers machined out of a copper plate. The heat exchangers were connected through a valve system to two constant-temperature baths (Haake A82). Each heat exchanger contained three loops through which the flow rate could be controlled independently. The temperatures of each heat exchanger were measured with three thermocouples epoxied separately into small-diameter holes, which were drilled close to the surface of the copper plate facing the fluid. In all experiments, the temperatures of each heat exchanger were uniform to within $\pm 0.2^\circ\text{C}$ of the desired temperature.

Measurement of the temperature distribution inside the test cell was made with 33 thermocouples with a wire diameter of 0.127 mm. They were placed in three different stainless steel rakes located at heights of 0.635, 2.38, and 4.125 cm measured from the bottom of the test cell. The rakes were positioned such that the temperatures were measured along the vertical centerplane of the test cell. The rake arms were oriented perpendicular to the flow direction (i.e., normal to the x - y plane) to minimize their influence on the flow field. Since the temperatures were essentially uniform over the depth of the

Table 1 Summary of experimental conditions ($A = 1.0$ $Pr = 0.0208$, $\alpha^* = 1.105$, $k^* = 1.0$, $\rho^* = 0.969$)

Experiment	$\Delta T_l, ^\circ\text{C}$	$\Delta T_s, ^\circ\text{C}$	S_T	Ra	Ste
1	10.2	4.8	0.468	3.275×10^5	5.074×10^{-2}
2	10.2	9.8	0.957	3.275×10^5	5.074×10^{-2}
3	10.2	19.8	1.935	3.275×10^5	5.074×10^{-2}
4	5.2	14.8	2.831	1.673×10^5	2.592×10^{-2}
5	15.2	14.8	0.971	4.877×10^5	7.557×10^{-2}

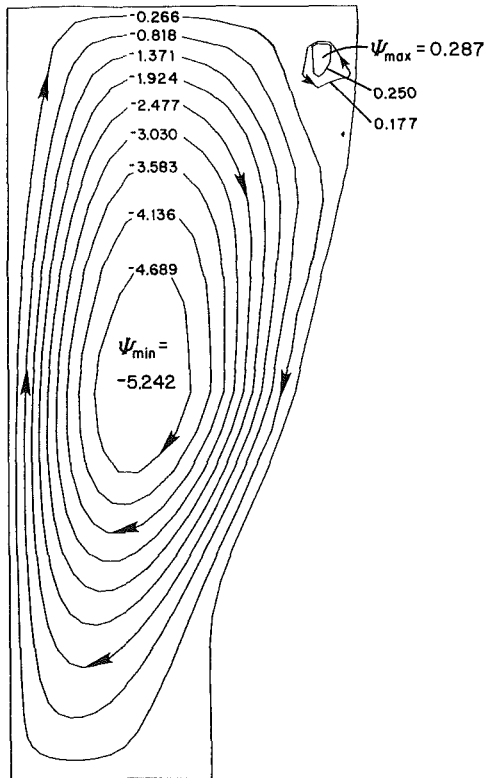


Fig. 2(a) Predicted streamlines

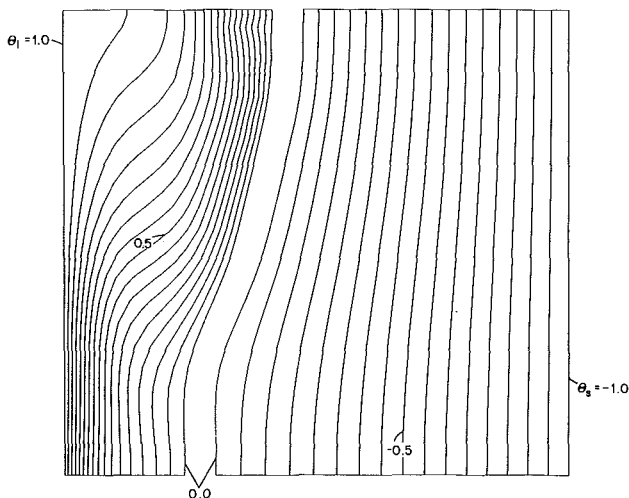


Fig. 2(b) Predicted isotherms (equal increments)

test cell, heat conduction along the rake arms can be expected to be negligibly small. The uncertainty in the location of each thermocouple bead was approximately ± 0.2 mm. All thermocouples were calibrated with an accuracy of $\pm 0.1^\circ\text{C}$. The thermocouples were connected to an HP-85 data-logger and

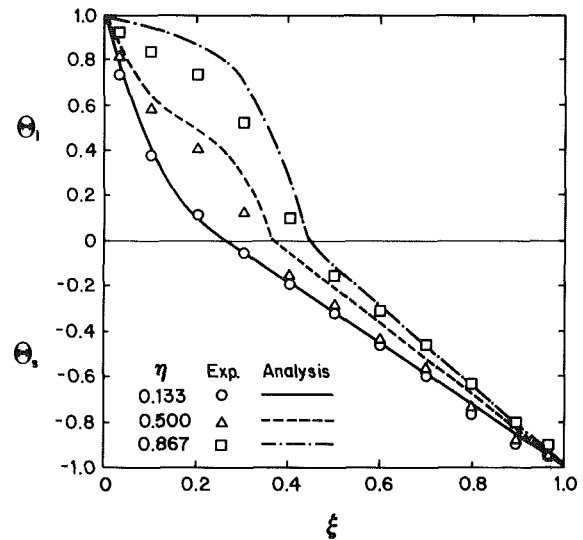


Fig. 2(c) Comparison of measured and predicted temperature profiles

Fig. 2 Results for Experiment 1 at $\tau = 0.0558$ ($t = 3$ min)

computer through which the temperatures could be measured and stored at preselected time intervals. The copper heat exchangers as well as the thermocouple rakes were protected from the liquid metal used as the phase-change material by a very thin coat of spray paint.

The phase-change material utilized in the experiments was 99.99 percent pure gallium. This metal is desirable as a test material mainly because of its low fusion temperature ($T_f = 29.78^\circ\text{C}$), enabling the experiments to be conducted close to ambient temperature, thereby reducing undesirable heat exchange with the surrounding through the Lexan and phenolic walls. In addition, the thermophysical properties of solid and liquid gallium are well documented (Cubberly, 1979). The highly anisotropic nature of the solid gallium crystals as well as the high cost of gallium of this purity are the two major disadvantages of using gallium as the phase-change material.

A total of five melting experiments was performed, covering a wide range of hot and cold wall temperatures (and, hence, a wide range of S_T and Ra). The experimental conditions together with the values of the dimensionless parameters are summarized in Table 1. All properties were evaluated at the mean temperatures of the liquid and the solid. The thermal conductivity of the solid gallium was obtained by taking an average of the values for the three crystal axes (Gau and Viskanta, 1986).

In preparing for each experiment, the test cell was filled with successive layers of liquid gallium, which were slowly solidified before more liquid was added. This was done to ensure a homogeneous structure of the solid in the test cell. Volume change during phase-change (gallium contracts by about 3 percent upon melting) was accommodated by allowing liquid gallium to enter the test cell through a small hole drilled

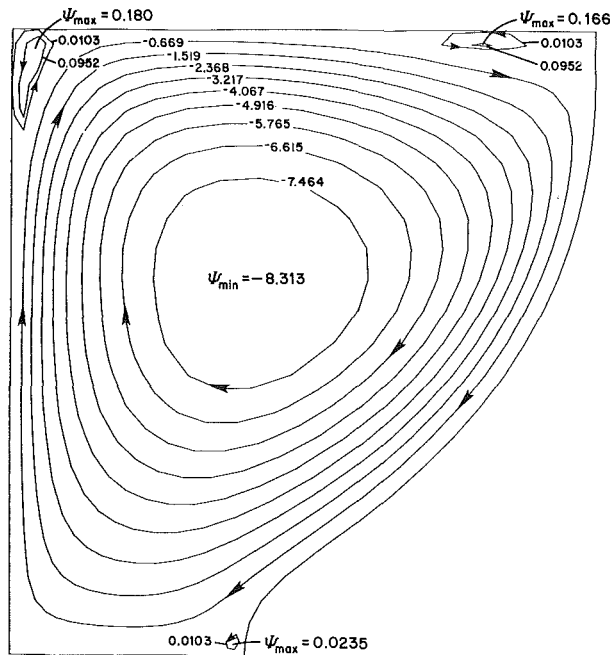


Fig. 3(a) Predicted streamlines

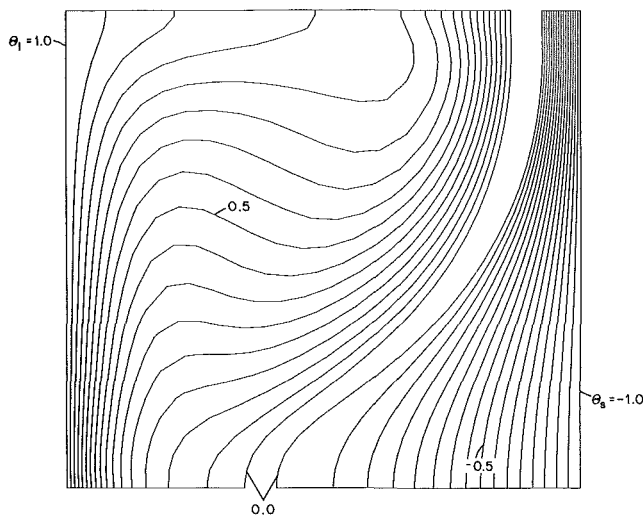


Fig. 3(b) Predicted Isotherms (equal increments)

in the top plate. In order to obtain uniform initial temperature of the solid, the water from the cold constant temperature bath was circulated through both heat exchangers for at least 5 h. In the meantime, the temperature of the hot constant temperature bath was maintained at T_H . The experiment was initiated by switching the left heat exchanger from the cold to the hot constant temperature bath. Due to the thermal inertia of the system and the large heat flux at the hot wall during the initial period of the melting experiment, it took approximately 20 s for the left heat exchanger to reach the temperature desired as the boundary condition.

The solid/liquid interface positions during the melting experiments were determined by interpolating the fusion temperature from the thermocouple readings. Since the horizontal distance between two thermocouple junctions was 4.75 mm, the error in the calculated interface location was estimated to be less than 2 mm. The accuracy of this method was also tested using a dip-stick to measure the solid/liquid interface positions. For this purpose, an L-shaped glass rod with a pointed tip was connected to an x - y measurement system.

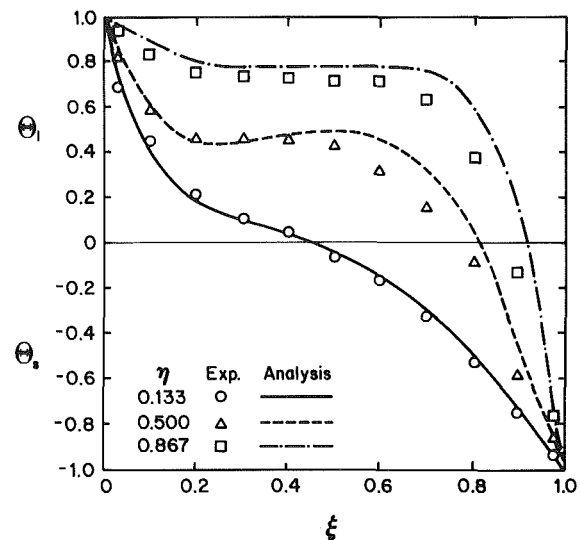


Fig. 3(c) Comparison of measured and predicted temperature profiles

Fig. 3 Results for Experiment 1 at $\tau = 0.1857$ ($t = 10$ min)

Good agreement with values interpolated from simultaneous temperature measurements was found.

Results and Discussion

Experiment 1. The numerical and experimental results for Experiment 1 are presented in detail in this section, which is followed by a discussion and comparison of the other experiments. The streamlines, isotherms, and temperature profiles at $\tau = 0.0558$ ($t = 3$ min), 0.1857 (10 min), and 0.9275 (50 min) are shown in Figs. 2, 3, and 4, respectively. In order to illustrate small recirculations in the corners of the melt region, two additional streamlines with values close to zero were plotted in Figs. 2(a), 3(a), and 4(a). Because the increments between these two streamlines are not the same as the constant increment for the other streamlines in the boundary layer and core regions, the spacings of the streamlines in the corners represent different mass flow rates. The time evolutions of the Nusselt numbers and the dimensions melt volume are presented in Figs. 5 and 6, respectively. Also shown in Figs. 5 and 6 are the corresponding curves for the limiting case of no fluid flow (i.e., $Ra = 0$) and zero solid subcooling (i.e., $S_T = 0$).

In Experiment 1, the melting process can be divided into four successive regimes:

- an initial pure conduction regime, during which the solid/liquid interface moves parallel to the hot wall;
- a regime characterized by developing convection in the upper portion of the liquid region and pure conduction in the lower portion; consequently, the interface exhibits a strong curvature in the upper portion and remains vertical in the lower portion;
- a convection-dominated regime, during which the entire interface is curved and moves faster in the upper than in the lower portion;
- and, finally, a regime during which the melting process is significantly influenced by heat extraction from the cold wall; melting takes place primarily in the lower portion of the enclosure and the interface reaches, eventually, a stationary position almost parallel to the cold wall.

The first two regimes are very similar to what has been observed in melting of a pure metal without solid subcooling (Webb and Viskanta, 1986) and of an ordinary nonmetallic solid with solid subcooling (Bernard et al., 1986). As can be seen from Figs. 5 and 6, the melting and heat transfer processes during the initial conduction regime follow very closely

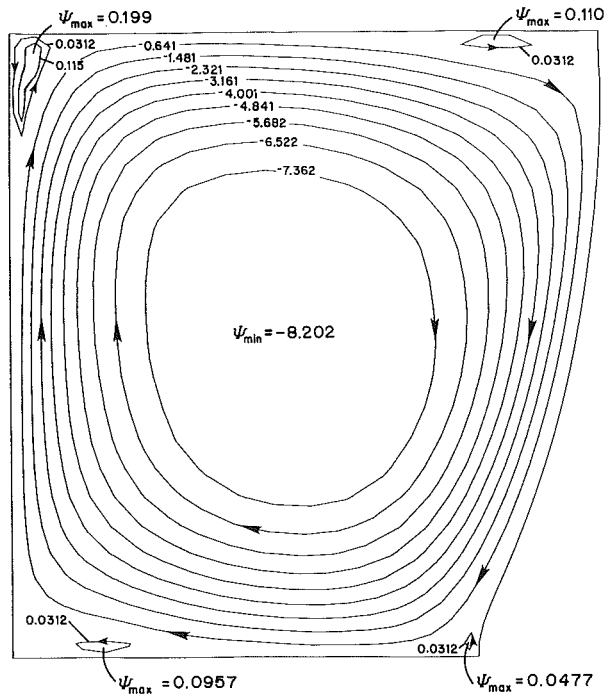


Fig. 4(a) Predicted streamlines

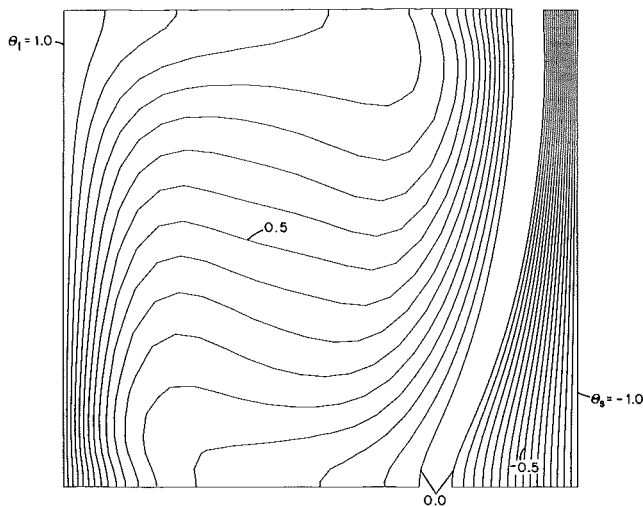


Fig. 4(b) Predicted isotherms (equal increments)

the analytical solution for the limiting case of $Ra = S_T = 0$. Figures 2(a) and 2(b) show typical streamlines and isotherms, respectively, for the second regime at $\tau = 0.0558$ ($t = 3$ min). Natural convection encompasses the upper three quarters of the melt region, with thermal boundary layers present along the hot wall and the (now) curved solid/liquid interface. In the lower quarter, however, the isotherms as well as the interface are almost vertical, indicating conduction-dominated heat transfer. Note the presence of a weak secondary recirculation cell in the upper right corner of the melt region. Such recirculation cells (see also Figs. 3a and 4a) are typical for natural convection of low Prandtl number fluids (i.e., liquid metals) and have been observed in other studies (Webb and Viskanta, 1986; Wolff and Viskanta, 1987; Wolff et al., 1988).

The second regime ends shortly after $\tau = 0.558$ (Fig. 2) when the convection region has expanded all the way to the bottom of the enclosure. Figure 5 shows that at this time, the average Nusselt number at the hot wall reaches a local minimum. The relatively small values of the Nusselt number at the cold wall

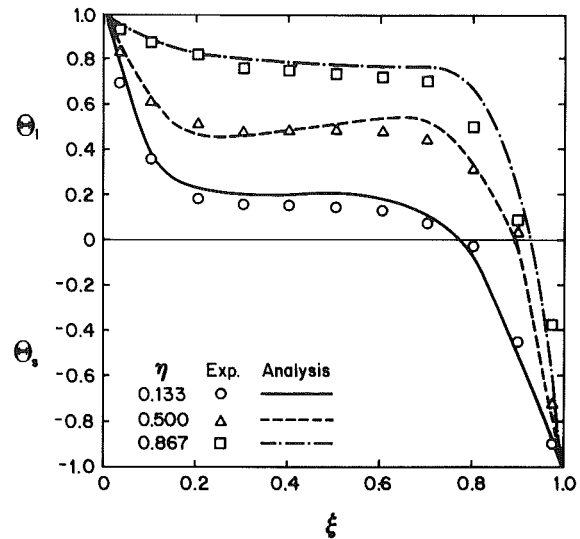


Fig. 4(c) Comparison of measured and predicted temperature profiles

Fig. 4 Results of Experiment 1 at $\tau = 0.9275$ ($t = 50$ min)

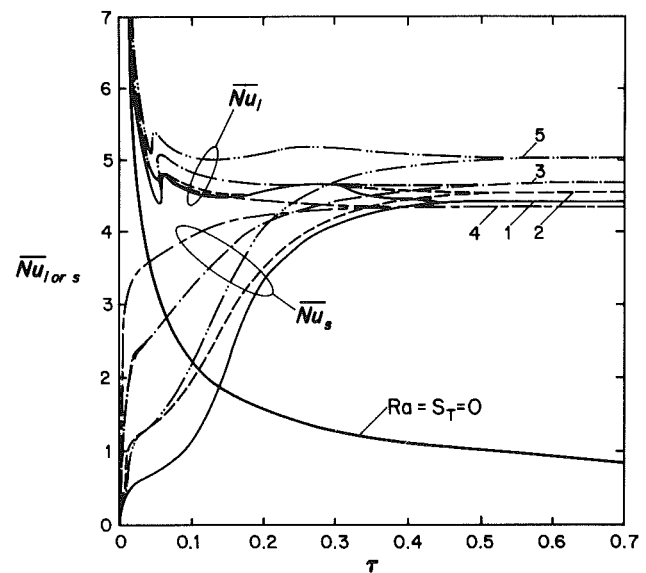


Fig. 5 Predicted time evolution of the average Nusselt numbers at the hot and cold walls

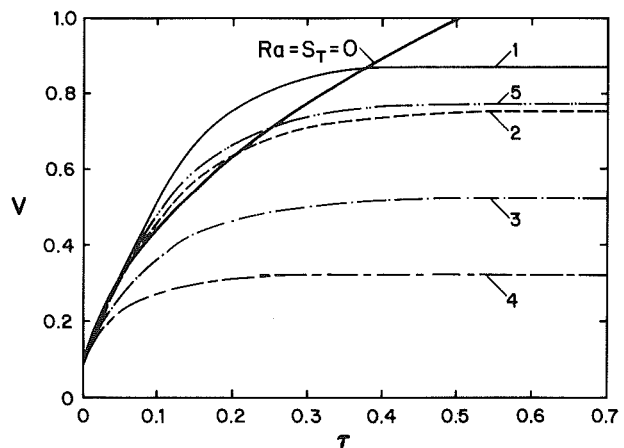


Fig. 6 Predicted time evolution of the melt volume

indicate that heat extraction from the cold wall and, hence, solid subcooling has only little influence on the melting process during the first two regimes in Experiment 1. Despite the presence of natural convection during the second regime, an examination of Fig. 6 reveals that the melt volume at the end of the second regime ($\tau=0.06$) is almost identical to the one for the case of $Ra=S_T=0$. Again, similar observations have been made in studies of melting of metals without solid subcooling (Webb and Viskanta, 1986, Wolff and Viskanta, 1987).

During the third regime, natural convection takes place in the entire melt region. Because the temperature of the liquid metal decreases as it flows down the solid/liquid interface, the temperature gradients and, hence, the melting rates are larger in the upper than in the lower portion of the enclosure. This results in a smoothly curved interface, intersecting the adiabatic top and bottom walls at right angles.

Figures 3(a) and 3(b) show the predicted streamlines and isotherms, respectively, at $\tau=0.1857$ ($t=10$ min), close to the end of the third regime. Thermal boundary layers are present along the hot wall and the interface, while weak recirculation cells can be observed in both the upper and the lower right corners of the melt region. The interface in the upper right third of the enclosure is now very close to the cold wall, resulting in large temperature gradients in the solid in this region. Due to the strong curvature of the interface, the horizontal extent of the solid region at the bottom of the enclosure is still large ($s(\eta=0)\approx 0.36$) and the temperature gradients in the solid are relatively small. The Nusselt number at the hot wall (Fig. 5) decreases slightly from a value of 4.8 at the beginning ($\tau=0.06$) to 4.5 at the end ($\tau=0.18$) of the third regime. On the other hand, the Nusselt number at the cold wall increases sharply (from 0.75 to 2.6), indicating that the melting process is increasingly influenced by heat conduction through the solid. Figure 6 shows that in the third regime, the dimensionless melt volume increases at a higher rate than for the limiting case of $Ra=S_T=0$. It is well known (Webb and Viskanta, 1986) that in convection-dominated melting without solid subcooling, the melt volume increases almost linearly with time. However, for the present case ($S_T=0.468$), the melt volume (V) versus time (τ) curve increasingly departs from an initially linear behavior. At the end of the third regime ($\tau=0.18$), the average melting rate (i.e., $dV/d\tau$) has decreased again to almost the same value as for $Ra=S_T=0$. In other words, the effect of solid subcooling on the melting process in Experiment 1 is significant during the later stages of the third regime. However, the general natures of the convection and melting processes remain similar to the ones without solid subcooling until the end of the third regime. As will be discussed in the next section, the above observations are only true for Experiment 1 and, hence, relatively small values of the subcooling parameter ($S_T<0.5$).

On the other hand, the fourth regime is unique to melting with solid subcooling. Due to the small extent of the solid in the upper portion of the cavity, the heat transfer rates through the liquid and solid are now balanced, so that the solid/liquid interface does not move. In the lower portion, however, the interface continues to move, because the horizontal extent of the solid is larger, while the temperature gradients in the solid are smaller than in the upper region. Consequently, the interface becomes increasingly vertical and parallel to the cold isothermal wall, as the system approaches steady state. The streamlines and isotherms at $\tau=0.9275$ ($t=50$ min) are shown in Figs. 4(a) and 4(b), respectively. At this time, the interface has reached a stationary position and the heat transfer rates through the liquid and solid are equal. The natural convection patterns in the liquid region are very similar to the ones for a vertical square cavity (Wolff et al., 1988). The interface still exhibits a slight curvature, because the natural convection flow downward along the interface causes a variation in the

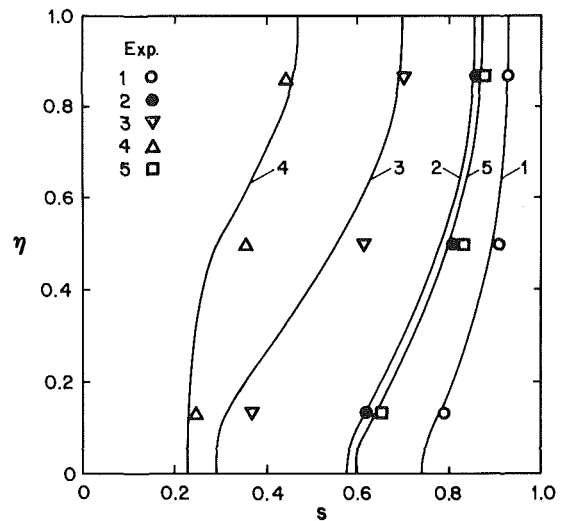


Fig. 7 Comparison of measured and predicted steady-state interface positions

local heat transfer rates. Figure 5 shows that the Nusselt number at the hot wall stays approximately constant throughout the third and fourth regimes (there is a slight maximum at about $\tau=0.3$), while the Nusselt number at the cold wall continues to increase until it approaches the same value as \bar{Nu}_h (at approximately $\tau=0.45$). Similarly, the melt volume (Fig. 6) slowly approaches its steady-state value.

Comparison of Predictions With Experiments. As a representative example, comparisons between the predicted and measured temperatures are presented for Experiment 1 at $\tau=0.0558$, 0.1857, and 0.9275 in Figs. 2(c), 3(c), and 4(c), respectively. Comparisons between predicted and measured solid/liquid interface positions at steady state are shown for all experiments in Fig. 7. In general, the experimental data agree with the predicted temperatures to within about 5 percent of the total temperature difference across the test cell. It is believed that most of the discrepancies can be attributed to experimental uncertainties, including inaccuracies in the thermocouple locations and readings as well as imperfect boundary conditions (isothermal and adiabatic). It can be observed that at all times the measurements indicate a lower intensity of natural convection in the melt region than predicted, which can be attributed to the presence of the thermocouple rake in the test cell. The discrepancies in the steady-state interface positions (Fig. 7) are well within the experimental uncertainties associated with the present measurement technique (see Experiments). It can be said that more accurate measurement techniques are needed to validate the predictions fully. In particular, measurements of the velocities in the liquid metal would be highly desirable for verifying the predicted flow patterns.

Uncertainties in the numerical predictions are primarily due to an insufficiently fine grid and the neglect of three-dimensional natural convection structures. Minor inaccuracies may be due to the neglect of density change upon melting and of thermophysical property variations with temperature. However, the good agreement between the measured and predicted melting rates and temperature distributions established some confidence in the numerical results.

Effects of Rayleigh Number and Solid Subcooling. Comparisons of the predicted average Nusselt numbers, dimensionless melt volume, and steady-state interface positions in Experiments 1 to 5 are shown in Figs. 5, 6, and 7, respectively. An examination of the results for Experiments 1, 2, and 3 reveals the effect of different subcooling parameters (S_T) on the melting process at the same Rayleigh number. The time

evolution of the Nusselt number at the hot wall (\overline{Nu}_h) in Experiments 2 and 3 follows quite closely the one for Experiment 1 (see Fig. 5). On the other hand, with increasing S_T , the Nusselt number at the cold wall (\overline{Nu}_c) increases at a much faster rate, indicating that for large S_T ($S_T \geq 2$), the influence of solid subcooling on the melting process is important almost from the beginning during all melting regimes. As expected, the melting rates decrease drastically with increasing S_T . In Experiment 2, the melting rate for the first three regimes is almost the same as for $Ra = S_T = 0$, while in Experiment 3, the melting rate is, except for the first conduction regime, smaller than for $Ra = S_T = 0$ (see Fig. 6). It should be noted that for the three experiments, the first two melting regimes (see Experiment 1) are of approximately the same duration. However, for large S_T (e.g., Experiment 3) a distinction between the third and fourth regime cannot be made, because of the strong influence of solid subcooling in both of these regimes. As in Experiment 1, the average Nusselt numbers at the hot wall (\overline{Nu}_h) stay approximately constant during the third and fourth regimes of Experiments 2 and 3, indicating that natural convection is quasi-steady. Steady-state is in all three experiments at approximately the same time ($\tau = 0.45$). With increasing S_T , the final melt volume decreases, while the steady-state interface (Fig. 7) becomes more curved. The latter is due to the fact that for large subcooling the steady-state interface is at a relatively large distance from the isothermal cold wall and, hence, its shape is more influenced by the natural convection in the liquid. It is also interesting to note the slight increase of the steady-state Nusselt number with increasing S_T and, hence, decreasing steady-state melt volume. This indicates that for natural convection in liquid metals, the Nusselt number increases only slightly with increasing "aspect ratio" (of the melt volume) (see also Wolff et al., 1988). The steady-state characteristics of the melting experiments are discussed in more detail in the next section.

A comparison of Experiments 2 and 5 shows the effect of increasing Rayleigh number (Ra) on the melting process at approximately the same value of the subcooling parameter ($S_T \approx 0.96$). Because it was impossible to vary the Rayleigh number in the present experiments by more than a factor of about three, the results for the two experiments are quite similar. However, it can be observed that both the melt volume and the Nusselt number at the cold wall increase at a faster rate for a higher Rayleigh number (see Figs. 5 and 6). As expected, the Nusselt number at the hot wall is at all times higher for a higher Rayleigh number.

The results of Experiments 4 reveal the effects of a very large value of the subcooling parameter ($S_T = 2.831$). The shape of the interface in steady-state (Fig. 7) suggest that for such large subcooling of the solid, the melting process never goes through the third and fourth (convection dominated) regimes. The melt volume stays small so that natural convection can develop only in the upper portion of the melt region, and the interface in the upper portion remains practically vertical throughout the experiment. In other words, Experiment 4 reaches a steady state approximately in the middle of the second regime. Because natural convection does not develop fully, Experiment 4 also has the smallest Nusselt number at steady state.

The above discussion shows that the melting process in the present experiments consists of a number of distinct regimes. However, the physical nature of each regime varies considerably for different amounts of solid subcooling. Although attempts have been made to identify the various regimes, it has not been possible to correlate the present results (i.e., \overline{Nu} and V) as functions of the relevant dimensionless parameters. Such correlations would involve consideration of each regime separately and matching of the functional relationships between the regimes. It cannot be expected that a single relation can be obtained for the entire melting process and reasonable

ranges of S_T and Ra . While for small solid subcooling, some of the results obtained for $S_T = 0$ (Webb and Viskanta, 1986) can be applied to the first three regimes (see Experiment 1), correlations for the steady-state behavior are presented in the following section.

Steady-State Characteristics. Assuming that at steady state the solid/liquid interface is (almost) vertical, integration of the interfacial energy balance, equation (7), over the height of the cavity (with $v_n = 0$) results in

$$V|_{\text{final}} = 1 - \frac{c_1 k^* S_T}{\overline{Nu}_l|_{\text{final}}} \quad (11)$$

The factor c_1 has been added in equation (11) in order to correct for the curvature of the steady-state interface (see Fig. 7). With $c_1 = 1.19$, equation (11) correlates the final melt volumes for Experiments 1, 2, and 5 to within 0.5 percent. For Experiment 3 ($S_T = 1.935$), the relative error increases to about 3 percent, while equation (11) is not applicable to Experiment 4. The large increase in the error for $S_T > 2$ can be attributed to the strong curvature of the interface as well as to the small value of $V|_{\text{final}}$, both of which cause a large departure from the assumption of one-dimensional conduction in the solid. According to equation (11), the subcooling parameters S_T must be less than \overline{Nu}_l/k^* for melting to take place (i.e., for the final melt volume to be greater than zero). It is also interesting to note that equation (11) can be utilized to estimate the average Nusselt number at steady-state, if the final melt volume is known (e.g., through measurements).

An attempt has been made to correlate the steady-state average Nusselt number ($\overline{Nu}_l|_{\text{final}}$) as a function of the dimensionless parameters that govern the natural convection heat transfer in the liquid region. According to Bejan (1984), in the boundary layer regime the Nusselt number for $Pr < 1$ scales such that the following correlation can be written:

$$\overline{Nu}_l|_{\text{final}} = c_2 (RaPr)^{1/4} \quad (12)$$

With $c_2 = 0.5$, equation (12) correlates the results for Experiments 1, 2, 3, and 5 to within 3 percent. Equation (12) is not applicable to Experiment 4, because natural convection is not in the boundary layer regime. The good fit of the present data with the above correlation indicates that the average Nusselt number is not strongly influenced by the curvature of the interface as well as by the different "aspect ratios" of the liquid regions at steady state. As can be seen from Fig. 5, equation (12) should also provide a good estimate of \overline{Nu}_l throughout the third and fourth regimes in Experiments 1, 2, 3, and 5, because natural convection during these regimes is quasi-steady. The Prandtl number dependence has been checked with data obtained for natural convection of tin ($Pr = 0.011$) in a vertical square enclosure (Wolff et al., 1988) and excellent agreement with the above correlation has been found. Good agreement has also been found with quasi-steady Nusselt numbers obtained for natural convection melting of gallium without solid subcooling (Webb and Viskanta, 1986). Note that substitution of equation (12) into (11) results in a correlation for the final melt volume that is a function of known parameters only.

Conclusions

A study has been performed of natural convection melting of a pure metal with subcooling of the solid. The numerical predictions are verified through a number of experiments, covering a range of Rayleigh numbers and subcooling parameters. It is found that the melting process consists of a sequence of four regimes and eventually approaches a steady state. For small solid subcooling, the first three regimes are found to be similar to the ones observed in melting without subcooling, while for moderate subcooling ($S_T \approx 1$) significant

differences can already be observed after the first two regimes. Large values of the subcooling parameter ($S_T > 2$) result in an early termination of the melting process and the last two regimes may never take place. It is shown that natural convection and solid subcooling have a considerable influence on melting of a metal. While many aspects of natural convection melting with solid subcooling appear to be similar for high and low Prandtl number fluids, important differences in the local flow structures and heat transfer mechanisms have been identified. It is concluded that additional research is necessary to arrive at general correlations for the dependence of the average Nusselt numbers and the melting rate on the governing dimensionless parameters. For moderate values of the subcooling parameter ($S_T < 2$), equations have been derived that accurately correlate the steady-state melt volume and heat transfer rates in the present system. Additional analyses and experiments are also needed to investigate the effects of different aspect ratios and a wider Rayleigh number range on melting of metals in enclosures.

Acknowledgments

The work reported in this paper was supported, in part, by the National Science Foundation under Grant No. CBT-8313573. Computer facilities were made available by Purdue University Computing Center.

References

- Bejan, A., 1984, *Convection Heat Transfer*, Wiley, New York.
- Benard, C., Gobin, D., and Zanoli, A., 1986, "Moving Boundary Problem: Heat Conduction in the Solid Phase of a Phase-Change Material During Melting Driven by Natural Convection in the Liquid," *International Journal of Heat and Mass Transfer*, Vol. 29, pp. 1669-1681.
- Chiesa, F. M., and Guthrie, R. I. L., 1974, "Natural Convection Heat Transfer Rates During Solidification and Melting of Metals and Alloy Systems," *ASME JOURNAL OF HEAT TRANSFER*, Vol. 95, pp. 377-390.
- Cubberly, W. H., 1979, *Metal Handbook-Properties and Selection: Nonferrous Alloys and Pure Metals*, 9th ed., ASM, Metals Park, OH, pp. 811-814.
- DeVahl Davis, G., and Jones, I. P., 1983, "Natural Convection in a Square Cavity: a Comparison Exercise," *International Journal of Numerical Methods in Fluids*, Vol. 3, pp. 227-248.
- Gau, C., and Viskanta, R., 1986, "Melting and Solidification of a Pure Metal on a Vertical Wall," *ASME JOURNAL OF HEAT TRANSFER*, Vol. 108, pp. 174-181.
- Hsu, C. F., 1982, "A Curvilinear-Coordinate Method for Momentum, Heat, and Mass Transfer in Domains of Irregular Geometry," Ph.D. Thesis, University of Minnesota, Minneapolis, MN.
- Kassinis, A., and Prusa, J., 1986, "Effects of Density Change and Subcooling on the Melting of a Solid in a Rectangular Enclosure," *Proceedings, 8th International Heat Transfer Conference*, U. Grigull et al., eds., Hemisphere, Washington, DC, pp. 1787-1792.
- Prusa, J., and Yao, L. S., 1985, "Effects of Density Change and Subcooling on the Melting of a Solid Around a Horizontal Heated Cylinder," *Journal of Fluid Mechanics*, Vol. 155, pp. 193-212.
- Sparrow, E. M., and Chuck, W., 1984, "An Implicit/Explicit Numerical Solution Scheme for Phase-Change Problems," *Numerical Heat Transfer*, Vol. 7, pp. 1-15.
- Sparrow, E. M., and Ohkubo, Y., 1986, "Numerical Analysis of Two-Dimensional Transient Freezing Including Solid-Phase and Tube-Wall Conduction and Liquid-Phase Natural Convection," *Numerical Heat Transfer*, Vol. 9, pp. 59-77.
- Szekely, J., and Chhabra, P. S., 1970, "The Effect of Natural Convection on the Shape and Movement of the Melt-Solid Interface in the Controlled Solidification of Lead," *Metallurgical Transactions B*, Vol. 1B, pp. 1195-1203.
- Viskanta, R., 1985, "Natural Convection in Melting and Solidification," in: *Natural Convection: Fundamentals and Applications*, S. Kakac et al., eds. Hemisphere, Washington, DC, pp. 845-877.
- Webb, B. W., and Viskanta, R., 1986, "Analysis of Heat Transfer During Melting of a Pure Metal From an Isothermal Vertical Wall," *Numerical Heat Transfer*, Vol. 5, pp. 539-558.
- Wolff, F., and Viskanta, R., 1987, "Melting of a Pure Metal From a Vertical Wall," *Experimental Heat Transfer*, Vol. 1, pp. 17-30.
- Wolff, F., Beckermann, C., and Viskanta, R., 1988, "Natural Convection of Liquid Metals in Vertical Cavities," *Experimental Thermal and Fluid Science*, Vol. 1, pp. 83-91.
- Yao, L. S., 1980, "Analysis of Heat Transfer in Slightly Eccentric Annuli," *ASME JOURNAL OF HEAT TRANSFER*, Vol. 102, pp. 279-284.